

THE DEPENDENCE OF THE IR-RADIO CORRELATION ON THE METALLICITY

JIANJIE QIU,^{1,2} YONG SHI,^{1,2} JUNZHI WANG,³ ZHI-YU ZHANG,⁴ AND LUWENJIA ZHOU^{1,2}

¹*School of Astronomy and Space Science, Nanjing University, Nanjing 210093, China.*

²*Key Laboratory of Modern Astronomy and Astrophysics (Nanjing University), Ministry of Education, Nanjing 210093, China.*

³*Shanghai Astronomical Observatory, Chinese Academy of Sciences, 80 Nandan Road, Shanghai 200030, China*

⁴*Institute for Astronomy, University of Edinburgh, Royal Observatory, Blackford Hill, Edinburgh EH9 3HJ, UK*

Submitted to ApJ

ABSTRACT

We have compiled a sample of 26 metal-poor galaxies with $12 + \log(\text{O}/\text{H}) < 8.1$ with both infrared continuum and 1.4 GHz radio continuum data. By comparing to galaxies at higher metallicity, we have investigated the dependence on the metallicity of the IR-radio relationship at 24 μm , 70 μm , 100 μm and 160 μm bands as well as the integrated FIR luminosity. It is found that metal-poor galaxies have on average lower q_{IR} than metal-rich ones with larger offsets at longer IR wavelengths, from -0.06 dex in $q_{24\mu\text{m}}$ to -0.6 dex in $q_{160\mu\text{m}}$. The q_{IR} of all galaxies as a whole at 160 μm show positive trends with the metallicity and IR-to-FUV ratio, and negative trends with the IR color, while those at lower IR wavelengths show weaker correlations. We proposed a mechanism that invokes combined effects of low obscured-SFR/total-SFR fraction and warm dust temperature at low metallicity to interpret the above behavior of q_{IR} , with the former reducing the IR radiation and the latter further reducing the IR emission at longer IR wavelength. Other mechanisms that are related to the radio emission including the enhanced magnetic field strength and increased thermal radio contribution are unable to reconcile the IR-wavelength-dependent differences of q_{IR} between metal-poor and metal-rich galaxies. In contrast to q_{IR} , the mean total-SFR/radio ratio of metal-poor galaxies is the same as the metal-rich one, indicating the 1.4 GHz radio emission is still an effective tracer of SFRs at low metallicity.

Keywords: infrared/radio correlation, galaxy: metal poor, dwarf galaxy, galaxy: star formation

1. INTRODUCTION

A tight linear correlation between radio emission (at the rest frequency of 1.4 GHz) and infrared (IR) emission was first established in 1980s for spiral galaxies (Helou et al. 1985; de Jong et al. 1985). The infrared emission is the re-radiation of the dust heated by UV radiation of massive stars. The radio emission is the synchrotron radiation of cosmic ray electrons as accelerated by shocks in Type II supernova (SN) remnants (Helou & Bicay 1993). At high radio frequency, the thermal radio emission from HII regions could also be an important component. As both IR and radio emission originate from star formation, the relation is widely utilized to study star formation activities (Condon et al. 2002; Murphy et al. 2006a,b) as well as an effective means to distinguish between star formation galaxies and AGN (Yun et al. 2001).

The IR-radio correlation spans five orders of magnitude in luminosity and holds for both late-type field star-forming galaxies (Yun et al. 2001) and low-mass Magellanic-type peculiar galaxies (Jurusik et al. 2014). Not only valid in the local universe, it also holds at high redshift up to $z \sim 1 - 3$ (Appleton et al. 2004; Sargent et al. 2010; Ivison et al. 2010a), although at high z in addition to the Synchrotron radiation, the energy loss due to the inverse Compton scatter off the cosmic microwave background may be important (Murphy 2009). Even with the stacking technique (See Ivison et al. 2010a for details), many works still found no redshift evolution of the correlation out to $z \sim 3$ (Ivison et al. 2010a,b; Sargent et al. 2010; Mao et al. 2011).

However, outliers to the relation do exist, including both radio-excess and radio-deficient (or FIR-excess) ones. The global FIR/radio ratio of cluster galaxies is found to be lower than that of field galaxies (Miller & Owen 2001; Murphy et al. 2009). It is proposed that the interaction between ISM and ICM produces shocklets to further accelerate CR electrons in the galaxy, enhancing the radio emission. Such radio-excess sources are also found in the massive cluster MS0451.6-0305 at $z \sim 0.54$ (Randriamampandry et al. 2015). To investigate the effect of tidal shocks created by galactic interactions and mergers, Donevski & Prodanović (2015) studied the trend of FIR/radio ratio with different merging stages for 43 infrared-bright star-forming interacting galaxies, and found a notable radio excess at some merger stages. They proposed that the radio excess is not only caused by the non-thermal radio emission from the gas bridge between interacting galaxies, but also by the emission of the CR electrons accelerated by shocks within individual interacting galaxies. At high- z , Smolčić et al. (2015) found radio excess in sub-millimeter galaxies at $z \sim 4 - 6$, which is argued to be caused by selection effects as these sources are at early stages of evolution. On the other hand, the radio-deficient galaxies are likely those star-bursts at very young stages where SN has not exploded yet while the dust emission could be present (Roussel et al. 2003).

In the past decade, due to the improved spatial resolution of the IR and radio observations, studies of the IR-radio relations are also carried out for spatially resolved nearby spiral galaxies. A series of works for a few dozens of galaxies were done by Murphy et al. (2006a,b, 2008, etc.) based on the observations with *Spitzer* Infrared Telescope and Westerbork Synthesis Radio Telescope (WSRT). By using the image-smearing technique (See Murphy et al. 2006a for details), they studied the cosmic-ray electron diffusion at sub-kpc scale, and showed that the FIR/radio ratio decreases with both the declining surface brightness and increasing radius.

Most of the previous studies, however, focused on star-forming galaxies around solar metal abundance, with few works for low-metallicity dwarf galaxies. The early investigations based on IRAS 60 μm and VLA 1.4 GHz detection of about 15 blue compact dwarf galaxies around $12 + \log(\text{O}/\text{H}) = 8.0$

indicate that the ratio of the two does not show systematic offsets from the spirals (Hopkins et al. 2002), and the derived SFRs from the two wavelengths agree with each other over five order of magnitudes. Investigations of a small sample of local group dwarfs did not find the offset in the $f_{60\mu\text{m}}/f_{2.64\text{GHz}}$ ratio from spiral galaxies either (Chyży et al. 2011). Another work about dwarf galaxies with *Spitzer* 24 μm and VLA 1.4 GHz detection shows the deviation of q_{24} at low metallicity from spirals (Wu et al. 2008). They found that above $12 + \log(\text{O}/\text{H}) = 8.0$ the q_{24} is almost constant while below $12 + \log(\text{O}/\text{H}) = 8.0$ the five out of six detection follows the decreasing trend with the decreasing metallicity, except for an outlier (SBS 0335-052E) that is even above the bulk of those spirals.

Metal-poor dwarf galaxies are far more numerous than massive galaxies and serves as the building blocks of massive galaxies at high- z . Extremely metal-poor galaxies ($12 + \log(\text{O}/\text{H}) < 7.6$) also offer an opportunity to study the galaxy evolution at the quasi-pristine metal environment (Shi et al. 2014, 2015, 2016). The IR-radio relation offers a powerful way to understanding a series of physical processes including star formation, dust heating, cosmic ray, magnetic field etc that happen in the interstellar medium (ISM) of galaxies (Schleicher & Beck 2016, e.g.). We would like to study the IR-radio relation of metal-poor galaxies and gain insights into the above physical processes in these galaxies. We will compile as many as dwarf galaxies with $12 + \log(\text{O}/\text{H}) \leq 8.1$ in the archive of *Herschel* Space Observatory as well as previous IR missions, along with the radio data from the literature. The goal is to not only enlarge the dwarf sample to study the IR/radio relationship at low metallicity but also to investigate the IR/radio ratio at different IR wavelengths. In § 2 we present the sample and data. The results are shown in § 3. The discussions are presented in § 4. In § 5 we present the conclusions.

2. SAMPLE SELECTION AND DATA REDUCTION

2.1. Sample Selection

In order to construct a sample involving as many metal-poor dwarfs as possible, we went through all programs in the *Herschel* science archive of nearby galaxies ($z < 0.1$) and compiled a catalog of galaxies that have broad-band images as observed by *Herschel*. We then searched for the measurements of the oxygen nebular abundance in the literature and defined our metal-poor sample as galaxies with $12 + \log(\text{O}/\text{H}) \leq 8.1$. The metallicity measurements of this metal-poor sample are mainly based on the direct method, while a comparison sample of metal-rich galaxies mainly uses various strong line methods. The former has a high precision (0.1 dex) in contrast to the latter with large systematic uncertainties (~ 0.5 dex) (Moustakas et al. 2010). Since our study focuses on the metal-poor ones, we expect the results are not affected significantly by the abundance measurement error. To further increase the number of metal-poor galaxies, we included dwarf objects from Wu et al. (2008) and Klein et al. (1991). The radio 1.4 GHz continuum data were compiled from the literature through NED and VLA archive. The final sample as listed in Table 1 contains 26 galaxies with $12 + \log(\text{O}/\text{H}) \leq 8.1$. Figure 1 shows the distribution of the oxygen abundance of these galaxies.

For the high-metallicity comparison sample, we included galaxies above $12 + \log(\text{O}/\text{H}) = 8.1$ from *Spitzer* Infrared Nearby Galaxies Survey (SINGS) (Dale et al. 2007; Moustakas et al. 2010), the Key Insights on Nearby Galaxies: A Far-Infrared Survey with *Herschel* sample (KINGFISH) (Dale et al. 2012) and Dwarf Galaxies Survey (DGS) programs (Madden et al. 2013). We removed AGN identified through the optical emission line diagnostics and radio-loud AGN by Moustakas et al.

(2010), [Mendoza-Castrejón et al. \(2015\)](#) and [Best & Heckman \(2012\)](#). The presence of faint radio emission from the central black-holes is still possible in this comparison sample, but because our sample is well-resolved star-forming galaxies so that such emission should be a small fraction of the total radio emission and thus the q value should not be affected. The final comparison sample is listed in Table 3.

To reduce the systematic uncertainties in the IR photometry measurements for our metal-poor sources that are generally faint in the IR, we carried out the aperture photometry of the IR fluxes at 24, 70, 100, and 160 μm . The IR images were retrieved from the data archives of two telescopes including *Spitzer* Space Telescope and *Herschel* Space Observatory. These observations were mainly done in the programs of [Dale et al. \(2007, 2009, 2012\)](#) and [Rémy-Ruyer et al. \(2013\)](#). Aperture loss was corrected based on the point spread functions of each telescope at the corresponding wavelength. The final derived IR fluxes listed in Table 2 are consistent with the literature values within 20%, 25%, 29% and 41% at 24, 70, 100, and 160 μm , respectively. As Mrk 1499 has no *Spitzer* or *Herschel* data so that the IRAS 60 and 100 μm photometry were used to interpolate the 70 and 100 μm fluxes. For metal-rich sources, the IR photometry were collected from the literature. The GALEX far-UV data of both samples were retrieved from the NED. All photometry are listed in Table 1, Table 2 and Table 3.

2.2. Measurements of q parameter, SFRs

Following [Helou et al. \(1985\)](#), the IR-to-radio ratio is defined as $q_{\text{IR}} = \log\left(\frac{S_{\text{IR}}}{S_{1.4\text{GHz}}}\right)$, where S_{IR} is the monochromatic IR flux at a given IR wavelength or the total FIR flux, and $S_{1.4\text{GHz}}$ is the 1.4 GHz radio continuum emission. Both fluxes are in the unit of Jy. The total FIR luminosity is measured by $L_{\text{FIR}} = 4.63 \times 10^{-15} \times (8.3L_{24} + 2.7L_{70} + L_{160})$, where L_{FIR} was in unit of L_{\odot} with L_{24} , L_{70} , and L_{160} in W/Hz ([Symeonidis et al. 2008](#)). The FIR luminosity was then divided by the median frequency to have the FIR flux $S_{\text{FIR}} = \frac{L_{\text{FIR}}}{4\pi \times D^2 \times \nu_{85\mu\text{m}}}$ in Jy.

The SFR is derived by using the equation

$$\text{SFR} = 0.68 \times 10^{-28} L_{\nu}(\text{FUV}) + 2.14 \times 10^{-42} L(24 \mu\text{m}) \quad (1)$$

, where the $L_{\nu}(\text{FUV})$ is the FUV band luminosity in $\text{erg s}^{-1} \text{Hz}^{-1}$, the $L(24 \mu\text{m})$ is the 24 μm band luminosity in erg s^{-1} , and the unit of SFR is $M_{\odot} \text{yr}^{-1}$ ([Leroy et al. 2008](#)). The calibration of SFRs have systematic uncertainties up to about 0.3 dex. The initial mass function may change at low metallicity. The low opacity due to the low metallicity could also result in stronger UV radiation for massive stars so that the SFRs of metal-poor galaxies may be overestimated. However, since our main focus is about the q parameter which is the ratio of two observed fluxes, the systematic uncertainty of the SFR measurement should not affect our main results.

3. RESULT

3.1. q_{IR} parameter as a function of the oxygen abundance

Figure 2 shows the trend of q_{IR} as a function of the gas-phase oxygen abundance, including $q_{24\mu\text{m}}$, $q_{70\mu\text{m}}$, $q_{100\mu\text{m}}$ and $q_{160\mu\text{m}}$. The mean $q_{24\mu\text{m}}$ of our metal-rich ($12 + \log(\text{O}/\text{H}) > 8.1$) galaxies is 1.34 ± 0.05 as listed in Table 4 where the uncertainty is the error of the mean. This average is comparable to the literature value in [Wu et al. \(2008\)](#) but larger by 0.3 dex than the result of [Appleton et al. \(2004\)](#). As shown in the first panel, metal-poor galaxies with $12 + \log(\text{O}/\text{H}) < 8.1$

have an average q , excluding lower-limits, close to the mean q of our metal-rich galaxies. The entire sample shows no apparent trend between $q_{24\mu\text{m}}$ and the metallicity with a Kendall's rank correlation coefficient of only 0.16, inconsistent with what is found in Wu et al. (2008) who claimed a rough trend of decreasing $q_{24\mu\text{m}}$ with the reducing metallicity. As we included all sources from Wu et al. (2008), the difference is most likely caused by the small sample studied in Wu et al. (2008). Below $12 + \log(\text{O}/\text{H}) < 7.6$, there is some hint that the dispersion increases but the number of galaxies is very limited mainly because of few radio continuum detection of such galaxies. The $q_{24\mu\text{m}}$ of the extremely metal-poor galaxy SBS 0335-052E is boosted due to its prominent warm dust emission as its IR SED peaks around $24 \mu\text{m}$, while another extremely metal-poor galaxy IZw 18 instead has a value below the mean.

In the $q_{70\mu\text{m}}$ panel, the mean value of our metal-rich sample is close to the mean of the sample by Yun et al. (2001), still a bit larger than the value by Appleton et al. (2004). As listed in Table 4, the mean q_{70} of our metal-poor galaxies was lower than the mean of metal-rich ones by 0.26 ± 0.09 dex. Especially, SBS 0335-052E that shows exceptionally high $q_{24\mu\text{m}}$ now has $q_{70\mu\text{m}}$ lower than the mean value of metal rich galaxies ($12 + \log(\text{O}/\text{H}) > 8.1$). All galaxies together show a weak trend of $q_{70\mu\text{m}}$ that decreases with the reducing metallicity, with a correlation coefficient of 0.32.

The overall behavior of $q_{70\mu\text{m}}$ is also seen in the panels of $q_{100\mu\text{m}}$ and $q_{160\mu\text{m}}$. Compared to the case of $q_{70\mu\text{m}}$, the mean $q_{100\mu\text{m}}$ and $q_{160\mu\text{m}}$ of metal-poor galaxies are increasingly lower than those of metal-rich ones, by 0.44 ± 0.12 and 0.61 ± 0.13 dex, respectively. At both wavelengths, there exists rough correlations between q and the metallicity for all galaxies together, with correlation coefficients of 0.42 and 0.57 at $100 \mu\text{m}$ and $160 \mu\text{m}$, respectively. The last panel of Figure 2 shows that mean q_{FIR} of metal-poor galaxies is also lower than the mean value of metal-rich ones by 0.24 ± 0.09 dex.

3.2. q_{IR} parameter as a function of the IR luminosity and IR-to-FUV ratio

The drop in the q parameter for low-metallicity galaxies could be a result of the low dust content in these galaxies so that only a small fraction of radiation from massive stars is reprocessed by dust and re-emitted in the IR bands.

We first show the q_{IR} as a function of the IR luminosity in Figure 3. At $24 \mu\text{m}$, metal-poor galaxies are less luminous than metal-rich ones but still cover a large range from around 10^5 to $10^{10} L_{\odot}$, while the metal-rich ones have a luminosity range from 10^6 to $10^{11} L_{\odot}$. At three longer wavelengths, metal-poor galaxies also cover a large range from 10^6 to $10^{10} L_{\odot}$. Overall, there is no apparent dependence of q_{IR} on the IR luminosity, indicating the IR luminosity should not be the main driver of lower q of metal-poor galaxies. Bell (2003) investigated the dependence of q of 249 galaxies on the IR luminosity down to $10^8 L_{\odot}$, and found no systematic change in the q , consistent with our results that further extends the study to 10^5 - $10^6 L_{\odot}$.

Figure 4 shows the q_{IR} as a function of the IR to far-UV flux ratio at different IR wavelengths. On average metal-poor galaxies show lower IR/far-UV ratio than metal-rich galaxies, indicating lower dust extinction in metal-poor galaxies. There is a weak trend of decreasing $q_{24\mu\text{m}}$ with reduced $f_{24\mu\text{m}}/f_{\text{FUV}}$ for the entire sample, with a correlation coefficient of 0.22. Such a behavior is also seen in $q_{100\mu\text{m}}$ vs. $f_{100\mu\text{m}}/f_{\text{FUV}}$ and $q_{160\mu\text{m}}$ vs. $f_{160\mu\text{m}}/f_{\text{FUV}}$, with correlation coefficients of 0.25 and 0.42, respectively. Although there is no trend between $q_{70\mu\text{m}}$ vs. $f_{70\mu\text{m}}/f_{\text{FUV}}$, metal-poor galaxies on average have lower $f_{70\mu\text{m}}/f_{\text{FUV}}$ than metal-rich galaxies. These dependencies on the IR/FUV ratio indicates that the lower q_{IR} of metal-poor galaxies are associated with their smaller IR/far-UV ratio at the corresponding IR wavelength.

3.3. q_{IR} parameter as a function of the IR color

The IR SED is sensitive to many physical parameters such as dust temperature, the heating source and dust grain properties etc. It is already known that the dust IR SED of metal-poor galaxies are different from those metal-rich ones (Engelbracht et al. 2008; Rémy-Ruyer et al. 2013; Shi et al. 2014; Zhou et al. 2016). Previous investigations of the dependence of the q_{IR} value on the IR color do not reach conclusive results. For example, no trend is seen between $q_{24\mu\text{m}}$ vs. $f(60\mu\text{m})/f(100\mu\text{m})$ in the work of Wu et al. (2008), while the dependence has been found in the work of Hummel et al. (1988) for the $q_{100\mu\text{m}}$ as a function of the dust temperature, and in the work of Roussel et al. (2003) for the q_{FIR} with $f(60\mu\text{m})/f(100\mu\text{m})$.

Figure 5 plots q_{24} vs. IR color at different wavelengths including $f_{24\mu\text{m}}/f_{70\mu\text{m}}$, $f_{70\mu\text{m}}/f_{100\mu\text{m}}$ and $f_{100\mu\text{m}}/f_{160\mu\text{m}}$. Except for SBS 0335-052E, the short wavelength color $f_{24\mu\text{m}}/f_{70\mu\text{m}}$ of metal-poor galaxies bears an overall similar range to that of metal-rich ones. A weak positive correlation is seen between q_{24} and $f_{24\mu\text{m}}/f_{70\mu\text{m}}$ for the entire sample, with a correlation coefficient of 0.33. The second panel of Figure 5 shows that metal-poor galaxies have on average warmer $f_{70\mu\text{m}}/f_{100\mu\text{m}}$ color than metal rich ones but no apparent correlation between q_{24} and $f_{70\mu\text{m}}/f_{100\mu\text{m}}$. Actually the two galaxies with highest $f_{70\mu\text{m}}/f_{100\mu\text{m}}$ around 0.4 show almost the largest and smallest q_{24} , respectively. The above result confirms a previous finding of no relation between $q_{24\mu\text{m}}$ and $f(60\mu\text{m})/f(100\mu\text{m})$ (Wu et al. 2008). The last panel of Figure 5 illustrates some weak dependence of $q_{24\mu\text{m}}$ on the far-IR color $f_{100\mu\text{m}}/f_{160\mu\text{m}}$, with a correlation coefficient of 0.26.

Figure 6 investigates the dependence of $q_{70\mu\text{m}}$ on the above three IR color. A weak correlation is seen between $q_{70\mu\text{m}}$ and $f_{24\mu\text{m}}/f_{70\mu\text{m}}$, with a correlation coefficient of -0.34. Overall the metal-poor and metal-rich galaxies share the same range in $f_{24\mu\text{m}}/f_{70\mu\text{m}}$ as already mentioned in the above. At the same $f_{24\mu\text{m}}/f_{70\mu\text{m}}$, q_{70} is smaller for metal-poor galaxies as compared to metal-rich galaxies. The two metal-poor galaxies with highest $f_{24\mu\text{m}}/f_{70\mu\text{m}}$ show low q_{70} but not as extreme as expected if there is a relation. The dependence of q_{70} on the $f_{70\mu\text{m}}/f_{100\mu\text{m}}$ is very weak, with a correlation coefficient of -0.05. At the same color, metal-poor galaxies on average occupy lower $q_{70\mu\text{m}}$ regimes as compared to metal-rich ones. Among two metal-poor galaxies with highest $f_{70\mu\text{m}}/f_{100\mu\text{m}}$, only one shows lower q_{70} than the remaining all galaxies. The last panel shows no strong relation between $q_{70\mu\text{m}}$ and the far-IR color $f_{100\mu\text{m}}/f_{160\mu\text{m}}$, with a correlation coefficient of about -0.2.

Figure 7 shows the $q_{100\mu\text{m}}$ as a function of the above three IR color. The first panel indicates a weak dependence of q_{100} on the $f_{24\mu\text{m}}/f_{70\mu\text{m}}$, with a correlation coefficient of -0.42. At the same color, metal-poor galaxies show somewhat lower $q_{100\mu\text{m}}$ than the metal rich ones. The SBS 0335-052E with highest $f_{24\mu\text{m}}/f_{70\mu\text{m}}$ does not show the lowest q_{100} . In the second panel some stronger trend is present for the $q_{100\mu\text{m}}$ with the $f_{70\mu\text{m}}/f_{100\mu\text{m}}$, with a correlation coefficient of -0.53. The two galaxies with the highest $f_{70\mu\text{m}}/f_{100\mu\text{m}}$ do have lowest q_{100} among the whole sample. In the last panel, the dependence of q_{100} on the $f_{100\mu\text{m}}/f_{160\mu\text{m}}$ is weak with a correlation coefficient of -0.33.

The $q_{160\mu\text{m}}$ as a function of the IR color is shown in Figure 8. An inverse relation of $q_{160\mu\text{m}}$ with $f_{24\mu\text{m}}/f_{70\mu\text{m}}$ is present with a correlation coefficient of -0.63. The relation between $q_{160\mu\text{m}}$ and $f_{70\mu\text{m}}/f_{100\mu\text{m}}$ is also apparent, with a correlation coefficient of -0.43. The relationship between $q_{160\mu\text{m}}$ and $f_{100\mu\text{m}}/f_{160\mu\text{m}}$ is the strongest one with a correlation coefficient of -0.71, indicating that the low $q_{160\mu\text{m}}$ of metal poor galaxies is associated with their high $f_{100\mu\text{m}}/f_{160\mu\text{m}}$.

In a summary, for the whole sample including metal-rich and metal-poor galaxies, only $q_{160\mu\text{m}}$ shows good relationships with three IR color. Previous studies of metal-rich galaxies also found a relatively

tight relationship between q at long IR wavelength and the dust temperature (Smith et al. 2014). Our study further extends this into metal-poor galaxies.

4. DISCUSSION

Our multi-wavelength investigations of q_{IR} at 24 μm , 70 μm , 100 μm , 160 μm and total far-IR band indicate that the average values of all q_{IR} except for $q_{24\mu\text{m}}$ are reduced at $12 + \log(\text{O}/\text{H}) < 8.1$ as compared to those above $12 + \log(\text{O}/\text{H}) = 8.1$. At longer IR wavelengths from 24 μm to 160 μm , the offsets become larger and the trend of decreasing q_{IR} with the IR/FUV ratio and IR color becomes stronger. In the following, we discuss possible causes for the observed behavior of q_{IR} at low metallicity.

As shown in Fig. 4, low q_{IR} of metal-poor galaxies is associated with low IR-to-FUV ratio, especially at long wavelength (160 μm) where a relation of the decreasing q_{IR} with decreasing IR-to-FUV ratio is present. As argued below this low q is driven by a combined effect of low obscured-SFR/total-SFR ratio and warm dust color in metal-poor galaxies. Although statistical studies show that low-metallicity galaxies have on average similar dust-to-stellar mass ratio to metal-rich ones both globally and locally (Hunt et al. 2014; Zhou et al. 2016), the $f_{160\mu\text{m}}$ -to-FUV signals a low fraction of obscured SFR relative to total SFR. The low $f_{160\mu\text{m}}$ -to-FUV ratio results in that the portion of radiation from massive stars that is absorbed by dust and re-emitted in the IR is reduced in metal-poor galaxies so that a larger portion of radiation escape through far-UV photons. However, it is still not enough to explain the wavelength-dependent offsets of q , meaning that at longer IR wavelength the q of metal-poor galaxies is lower than metal-rich galaxies. This wavelength dependence needs to invoke the efficient dust heating that increase the IR emission at short wavelength, which is consistent with finding that the dust of metal-poor galaxies is in general warmer (Rémy-Ruyer et al. 2013; Zhou et al. 2016). The efficient dust heating is also consistent with the observed inverse relationship between q_{IR} and the IR color at long wavelength ($q_{160\mu\text{m}}$) as shown in Fig. 7 and Fig. 8. The above scenario implies that the SFR/radio ratio of metal-poor galaxies should be the same as that of metal-rich ones, which is demonstrated by our data as shown in Fig. 10. The mean value of $\log(\text{SFR}/L_{20\text{cm}})$ were -36.39 ± 0.1 and -36.39 ± 0.05 for metal-poor and metal-rich samples, respectively. Here we adopted the same SFR calibration for both samples. If any metallicity-dependent calibration exists, the result may change.

If the magnetic field is stronger in metal-poor galaxies, the 1.4 GHz synchrotron emission may be boosted to reduce their q values. The total field strength is measured by assuming equipartition between magnetic and cosmic-ray energy. Such equipartition magnetic field strength of spiral galaxies is around 10 - 20 μG as reviewed by Fletcher (2010), while gas-rich galaxies with high SFRs can have much higher strength up to 50 - 100 μG (Beck et al. 2005; Adebahr et al. 2013). The magnetic strength has been reported for some of our metal-poor sample. NGC 1569 was measured to have a strength of $14 \pm 3 \mu\text{G}$ (Kepley et al. 2010). The field strength of blue compact dwarf IZw 18 is about 11 μG or even higher if the emitting region is compact (Hunt et al. 2005). SBS 0335-052E has a field strength at least 30 μG (Hunt et al. 2004). IC 2574 is shown to have a weak strength about 4 μG (Chyży et al. 2007). Literature studies show that dwarfs can have a range of magnetic field of strength, $< 5 \mu\text{G}$ (Chyży et al. 2011) for dwarf irregulars and 2 - 6 times higher for blue compact dwarfs (Hunt et al. 2004, 2005). It is argued that the equipartition magnetic strength is proportional to the SFR surface density with a power index around 0.3 for both spiral and dwarf

galaxies (Niklas & Beck 1997; Chyży et al. 2011). The mechanisms may be related to the dynamo as driven by SFR-related events to amplify the field strength.

We test the deviation of the q_{IR} for our metal-poor galaxies from the mean value of metal-rich galaxies as a function of their SFR surface densities as shown in Figure 11. If magnetic fields play roles in lowering q of metal-poor galaxies, we should see q_{IR} at all IR wavelength decrease with the increasing SFR surface density, which is nevertheless not evident in the figure. At $24 \mu\text{m}$, the offset of q_{IR} shows some positive relationship with the SFR surface density with a correlation coefficient of 0.37. The offset of $q_{70\mu\text{m}}$ is almost independent with the SFR surface density, with a correlation coefficient of -0.16. Some inverse trends are seen in the $100 \mu\text{m}$ and $160 \mu\text{m}$ panels, with correlation coefficients of -0.48 and -0.46, respectively. All these behaviors are inconsistent with the scenario invoking the increased magnetic fields which should reduce q_{IR} with the same amount at all IR wavelengths. Instead the behavior seen in Figure 11 is consistent with the efficient dust heating at high SFR surface densities to increase the short wavelength emission while reducing the long wavelength radiation. As a result, Figure 11 indeed supports the scenario of low obscured SFR fraction and warm dust color of metal-poor galaxies that cause the low q_{IR} as discussed above. The median value of SFR surface densities of our metal-poor galaxies correspond to a magnetic field strength about $8 \mu\text{G}$ (Chyży et al. 2011), which is not larger than the typical value of spiral galaxies ($10\text{-}20 \mu\text{G}$, Fletcher (2010)), further supporting it is not the enhanced magnetic field strength that reduces the q of metal-poor galaxies. As compared to the theoretical model (Schleicher & Beck 2016), our SFR surface density is above the threshold (10^{-4} - $10^{-6} M_{\odot}/\text{yr}$) where the magnetic-field/SFR and cosmic diffusion loss may break down the IR-radio relationship of dwarf galaxies. In addition, Fig. 10 shows that, if the SFR calibration does not depend on the metallicity, metal-poor galaxies have similar SFR-to-radio ratio to metal-rich ones, also disfavoring the scenario of enhanced magnetic field strength.

The above discussions assume 1.4 GHz is dominated by non-thermal synchrotron emission. Compared to spiral galaxies, metal-poor dwarfs have a higher contribution from thermal emission, but usually no more than 30% at 1.4 GHz based on studies of individual galaxies as well as statistical studies (Niklas & Beck 1997; Hunt et al. 2004). The low obscured SFR fraction means that more ionized photons could escape to ionize a larger portion of gas, resulting in enhanced thermal emission from free electron. However, if the radio emission is elevated by 30% due to thermal contribution, the q_{IR} is reduced by only 0.1 dex, not enough to explain the observed offsets. And more over, such offsets should be IR wavelength independent, which is inconsistent with what is observed.

As a summary, metal-poor galaxies have lower q_{IR} as compared to metal-rich galaxies, with larger offsets in q_{IR} at longer IR wavelength, which could be explained by the combined effects of low obscured SFR fraction and warm dust temperature of metal-poor galaxies. Other mechanisms such as enhanced magnetic fields and enhanced thermal emission as discussed above, as well as others such as more powerful supernovae from more massive stars born in metal-poor gas are unable to reconcile the wavelength-dependent behavior of q_{IR} .

5. CONCLUSION

We have compiled a sample of 26 metal-poor galaxies at $12 + \log(\text{O}/\text{H}) \leq 8.1$ with multiple IR and radio 1.4 GHz photometry data. With a comparison sample of metal-rich galaxies at $12 + \log(\text{O}/\text{H}) > 8.1$, we perform studies of IR-radio relationships. Our main conclusions are the following:

1. The q_{IR} of metal-poor galaxies is lower than the metal-rich ones, with larger offsets at longer IR wavelengths. The mean offsets of metal-poor galaxies from metal-rich galaxies are -0.06 ± 0.13 , -0.26 ± 0.1 , -0.44 ± 0.12 , -0.61 ± 0.13 and -0.24 ± 0.1 for $q_{24\mu\text{m}}$, $q_{70\mu\text{m}}$, $q_{100\mu\text{m}}$, $q_{160\mu\text{m}}$ and q_{FIR} , respectively.
2. The drop in q_{IR} at long IR wavelength ($160 \mu\text{m}$) is related to the metallicity, the IR-to-FUV ratio and the IR color including $f_{24\mu\text{m}}/f_{70\mu\text{m}}$, $f_{70\mu\text{m}}/f_{100\mu\text{m}}$ and $f_{100\mu\text{m}}/f_{160\mu\text{m}}$.
3. The total SFR to radio ratio of metal-poor galaxies have a similar mean to that of metal-rich ones.
4. The plausible mechanism to explain the behavior of the q_{IR} of metal-poor galaxies invokes the combined effect of low obscured-SFR/total-SFR ratio and warm IR color. The former means less absorbed radiation from massive stars by dust and thus less re-emitted IR emission. The latter increases the short IR wavelength emission, in particular 24 micron, relative to longer wavelengths. Other mechanisms such as enhanced magnetic field strength and enhanced thermal contribution are difficult to explain the IR wavelength dependence of the behavior.

We thank the anonymous referee for helpful and constructive suggestions that improved the quality of the paper. J.Q., Y.S. and L.Z. acknowledges support for this work from the National Natural Science Foundation of China (NSFC grant 11373021) and the Excellent Youth Foundation of the Jiangsu Scientific Committee (grant BK20150014). This research has made use of the NASA/IPAC Extragalactic Database (NED) which is operated by the Jet Propulsion Laboratory, California Institute of Technology, under contract with the National Aeronautics and Space Administration.

REFERENCES

- Adebahr, B., Krause, M., Klein, U., et al. 2013, *A&A*, 555, A23
- Appleton, P. N., Fadda, D. T., Marleau, F. R., et al. 2004, *ApJS*, 154, 147
- Beck, R., Fletcher, A., Shukurov, A., et al. 2005, *A&A*, 444, 739
- Bell, E. F. 2003, *ApJ*, 586, 794
- Berg, D. A., Skillman, E. D., Marble, A. R., et al. 2012, *ApJ*, 754, 98
- Best, P. N., & Heckman, T. M. 2012, *MNRAS*, 421, 1569
- Brown, M. J. I., Moustakas, J., Smith, J.-D. T., et al. 2014, *ApJS*, 212, 18
- Cannon, J. M., & Skillman, E. D. 2004, *ApJ*, 610, 772
- Cannon, J. M., Walter, F., Skillman, E. D., & van Zee, L. 2005, *ApJL*, 621, L21
- Chyży, K. T., Bomans, D. J., Krause, M., et al. 2007, *A&A*, 462, 933
- Chyży, K. T., Weżgowiec, M., Beck, R., & Bomans, D. J. 2011, *A&A*, 529, A94
- Condon, J. J., Cotton, W. D., & Broderick, J. J. 2002, *AJ*, 124, 675
- Condon, J. J., Cotton, W. D., Greisen, E. W., et al. 1998, *AJ*, 115, 1693
- Dale, D. A., Aniano, G., Engelbracht, C. W., et al. 2012, *ApJ*, 745, 95
- Dale, D. A., Cohen, S. A., Johnson, L. C., et al. 2009, *ApJ*, 703, 517
- Dale, D. A., Gil de Paz, A., Gordon, K. D., et al. 2007, *ApJ*, 655, 863
- de Jong, T., Klein, U., Wielebinski, R., & Wunderlich, E. 1985, *A&A*, 147, L6
- Donevski, D., & Prodanović, T. 2015, *MNRAS*, 453, 638
- Engelbracht, C. W., Rieke, G. H., Gordon, K. D., et al. 2008, *ApJ*, 678, 804-827
- Esteban, C., García-Rojas, J., Carigi, L., et al. 2014, *MNRAS*, 443, 624
- Fletcher, A. 2010, *The Dynamic Interstellar Medium: A Celebration of the Canadian Galactic Plane Survey*, 438, 197
- Gil de Paz, A., Boissier, S., Madore, B. F., et al. 2007, *ApJS*, 173, 185
- Guseva, N. G., Izotov, Y. I., Fricke, K. J., & Henkel, C. 2012, *A&A*, 541, A115

- Guseva, N. G., Izotov, Y. I., Papaderos, P., & Fricke, K. J. 2007, *A&A*, 464, 885
- Guseva, N. G., Papaderos, P., Izotov, Y. I., et al. 2003, *A&A*, 407, 91
- Guseva, N. G., Papaderos, P., Izotov, Y. I., et al. 2003, *A&A*, 407, 105
- Guseva, N. G., Izotov, Y. I., & Thuan, T. X. 2000, *ApJ*, 531, 776
- Hao, C.-N., Kennicutt, R. C., Johnson, B. D., et al. 2011, *ApJ*, 741, 124
- Heckman, T. M., Robert, C., Leitherer, C., Garnett, D. R., & van der Rydt, F. 1998, *ApJ*, 503, 646
- Heeschen, D. S., & Wade, C. M. 1964, *AJ*, 69, 277
- Helou, G., & Bica, M. D. 1993, *ApJ*, 415, 93
- Helou, G., Soifer, B. T., & Rowan-Robinson, M. 1985, *ApJL*, 298, L7
- Hopkins, A. M., Schulte-Ladbeck, R. E., & Drozdovsky, I. O. 2002, *AJ*, 124, 862
- Hummel, E., Davies, R. D., Pedlar, A., Wolstencroft, R. D., & van der Hulst, J. M. 1988, *A&A*, 199, 91
- Hunt, L. K., Dyer, K. K., & Thuan, T. X. 2005, *A&A*, 436, 837
- Hunt, L. K., Testi, L., Casasola, V., et al. 2014, *A&A*, 561, A49
- Hunt, L. K., Dyer, K. K., Thuan, T. X., & Ulvestad, J. S. 2004, *ApJ*, 606, 853
- Hunter, D. A., van Woerden, H., & Gallagher, J. S., III 1994, *ApJS*, 91, 79
- Iverson, R. J., Alexander, D. M., Biggs, A. D., et al. 2010, *MNRAS*, 402, 245
- Iverson, R. J., Magnelli, B., Ibar, E., et al. 2010, *A&A*, 518, L31
- Izotov, Y. I., Papaderos, P., Guseva, N. G., Fricke, K. J., & Thuan, T. X. 2004, *A&A*, 421, 539
- Izotov, Y. I., Stasińska, G., Meynet, G., Guseva, N. G., & Thuan, T. X. 2006, *A&A*, 448, 955
- Izotov, Y. I., Chaffee, F. H., Foltz, C. B., et al. 1999, *ApJ*, 527, 757
- Izotov, Y. I., & Thuan, T. X. 1999, *ApJ*, 511, 639
- Izotov, Y. I., & Thuan, T. X. 1998, *ApJ*, 500, 188
- Izotov, Y. I., Thuan, T. X., & Lipovetsky, V. A. 1997, *ApJS*, 108, 1
- Izotov, Y. I., Thuan, T. X., & Lipovetsky, V. A. 1994, *ApJ*, 435, 647
- Izotov, Y. I., Thuan, T. X., & Stasińska, G. 2007, *ApJ*, 662, 15
- Jurusik, W., Drzazga, R. T., Jableka, M., et al. 2014, *A&A*, 567, A134
- Kepley, A. A., Mühle, S., Everett, J., et al. 2010, *ApJ*, 712, 536
- Kepley, A. A., Zweibel, E. G., Wilcots, E. M., Johnson, K. E., & Robishaw, T. 2011, *ApJ*, 736, 139
- Klein, U., Weiland, H., & Brinks, E. 1991, *A&A*, 246, 323
- Kobulnicky, H. A., & Johnson, K. E. 1999, *ApJ*, 527, 154
- Kobulnicky, H. A., Kennicutt, R. C., Jr., & Pizagno, J. L. 1999, *ApJ*, 514, 544
- Kobulnicky, H. A., & Skillman, E. D. 1997, *ApJ*, 489, 636
- Kong, X., Cheng, F. Z., Weiss, A., & Charlot, S. 2002, *A&A*, 396, 503
- López-Sánchez, Á. R., Esteban, C., & Rodríguez, M. 2004, *ApJS*, 153, 243
- Lee, H., & Skillman, E. D. 2004, *ApJ*, 614, 698
- Lee, H., Skillman, E. D., & Venn, K. A. 2006, *ApJ*, 642, 813
- Lee, J. C., Gil de Paz, A., Kennicutt, R. C., Jr., et al. 2011, *ApJS*, 192, 6
- Leroy, A., Bolatto, A. D., Simon, J. D., & Blitz, L. 2005, *ApJ*, 625, 763
- Leroy, A. K., Walter, F., Brinks, E., et al. 2008, *AJ*, 136, 2782
- Madden, S. C., Rémy-Ruyer, A., Galametz, M., et al. 2013, *PASP*, 125, 600
- Magrini, L., & Gonçalves, D. R. 2009, *MNRAS*, 398, 280
- Mao, M. Y., Huynh, M. T., Norris, R. P., et al. 2011, *ApJ*, 731, 79
- Masegosa, J., Moles, M., & Campos-Aguilar, A. 1994, *ApJ*, 420, 576
- Matthews, L. D., & Uson, J. M. 2008, *AJ*, 135, 291-318
- McCall, M. L., Rybski, P. M., & Shields, G. A. 1985, *ApJS*, 57, 1
- Mendoza-Castrejón, S., Dultzin, D., Krongold, Y., González, J. J., & Elitzur, M. 2015, *MNRAS*, 447, 2437
- Miller, N. A., & Owen, F. N. 2001, *AJ*, 121, 1903
- Moustakas, J., Kennicutt, R. C., Jr., Tremonti, C. A., et al. 2010, *ApJS*, 190, 233-266
- Muñoz-Mateos, J. C., Gil de Paz, A., Zamorano, J., et al. 2009, *ApJ*, 703, 1569-1596
- Murphy, E. J., Braun, R., Helou, G., et al. 2006, *ApJ*, 638, 157
- Murphy, E. J., Helou, G., Braun, R., et al. 2006, *ApJL*, 651, L111

- Murphy, E. J., Helou, G., Kenney, J. D. P., Armus, L., & Braun, R. 2008, *ApJ*, 678, 828-850
- Murphy, E. J., Kenney, J. D. P., Helou, G., Chung, A., & Howell, J. H. 2009, *ApJ*, 694, 1435
- Murphy, E. J. 2009, *ApJ*, 706, 482
- Niklas, S., & Beck, R. 1997, *A&A*, 320, 54
- Popescu, C. C., & Hopp, U. 2000, *A&AS*, 142, 247
- Pustilnik, S. A., Kniazev, A. Y., Pramskij, A. G., Ugryumov, A. V., & Masegosa, J. 2003, *A&A*, 409, 917
- Rémy-Ruyer, A., Madden, S. C., Galliano, F., et al. 2013, *A&A*, 557, A95
- Randriamampandry, S. M., Crawford, S. M., Cress, C. M., et al. 2015, *MNRAS*, 447, 168
- Roussel, H., Helou, G., Beck, R., et al. 2003, *ApJ*, 593, 733
- Sargent, M. T., Schinnerer, E., Murphy, E., et al. 2010, *ApJL*, 714, L190
- Saviane, I., Ivanov, V. D., Held, E. V., et al. 2008, *A&A*, 487, 901
- Schleicher, D. R. G., & Beck, R. 2016, *A&A*, 593, A77
- Shi, F., Kong, X., Li, C., & Cheng, F. Z. 2005, *A&A*, 437, 849
- Shi, Y., Armus, L., Helou, G., et al. 2014, *Nature*, 514, 335
- Shi, Y., Wang, J., Zhang, Z.-Y., et al. 2015, *ApJL*, 804, L11
- Shi, Y., Wang, J., Zhang, Z.-Y., et al. 2016, *Nature Communications*, 7, 13789
- Skillman, E. D., Côté, S., & Miller, B. W. 2003, *AJ*, 125, 610
- Smith, D. J. B., Jarvis, M. J., Hardcastle, M. J., et al. 2014, *MNRAS*, 445, 2232
- Smolčić, V., Karim, A., Miettinen, O., et al. 2015, *A&A*, 576, A127
- Storchi-Bergmann, T., Calzetti, D., & Kinney, A. L. 1994, *ApJ*, 429, 572
- Sulentic, J. W. 1976, *ApJS*, 32, 171
- Symeonidis, M., Willner, S. P., Rigopoulou, D., et al. 2008, *MNRAS*, 385, 1015
- Thuan, T. X., Hibbard, J. E., & Lévrier, F. 2004, *AJ*, 128, 617
- Thuan, T. X., & Izotov, Y. I. 2005, *ApJS*, 161, 240
- Thuan, T. X., Izotov, Y. I., & Lipovetsky, V. A. 1995, *ApJ*, 445, 108
- Ugryumov, A. V., Engels, D., Pustilnik, S. A., et al. 2003, *A&A*, 397, 463
- van Zee, L., Haynes, M. P., Salzer, J. J., & Broeils, A. H. 1996, *AJ*, 112, 129
- van Zee, L., & Haynes, M. P. 2006, *ApJ*, 636, 214
- Wu, Y., Charmandaris, V., Houck, J. R., et al. 2008, *ApJ*, 676, 970-977
- Yun, M. S., Reddy, N. A., & Condon, J. J. 2001, *ApJ*, 554, 803
- Zhou, L., Shi, Y., Diaz-Santos, T., et al. 2016, *MNRAS*, 458, 772

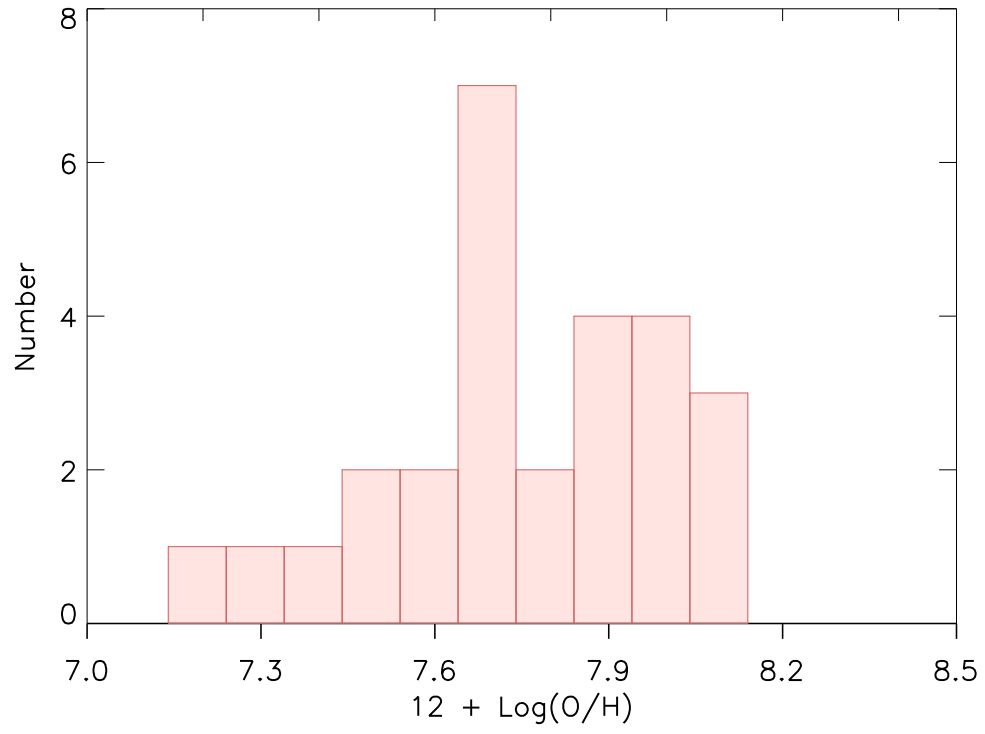


Figure 1. The distribution of the oxygen abundance $12 + \log(\text{O}/\text{H})$ of our compiled metal-poor galaxies.

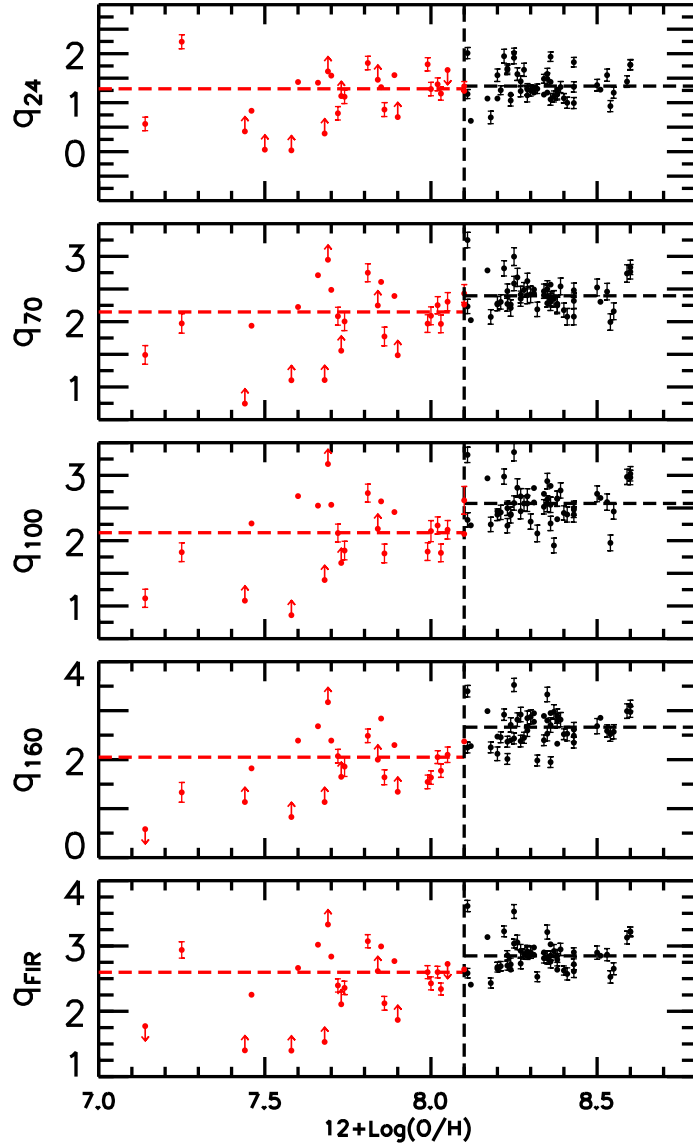


Figure 2. The q_{IR} as a function of the oxygen abundance at $24\mu\text{m}$, $70\mu\text{m}$, $100\mu\text{m}$, $160\mu\text{m}$, and FIR (definition at Section 2). The red points denote metal-poor galaxies and black points are for metal-rich galaxies. The vertical dashed line represents the value of $12 + \log(\text{O}/\text{H}) = 8.1$, while two horizontal dashed lines indicate the average values of metal-poor and metal-rich galaxies, respectively.

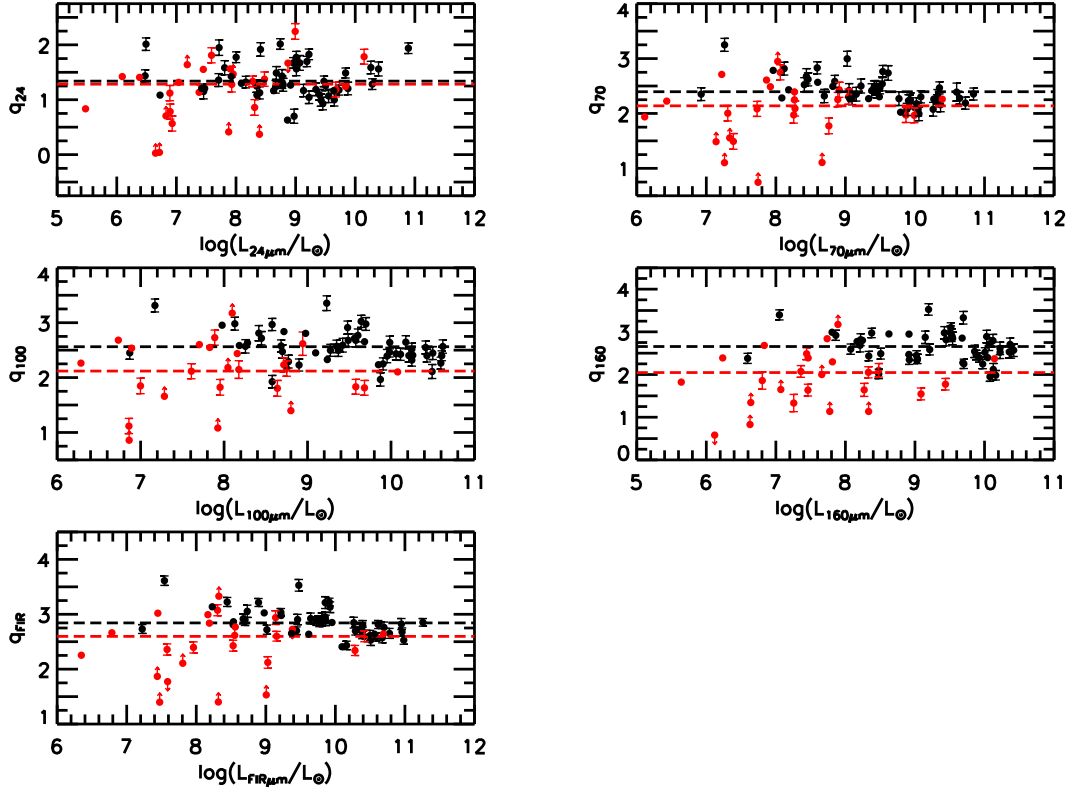


Figure 3. The q_{IR} as a function of the IR luminosity. The red points denote metal-poor galaxies and black points are for metal-rich galaxies. The two horizontal dashed lines indicate the average values of metal-poor and metal-rich galaxies, respectively.

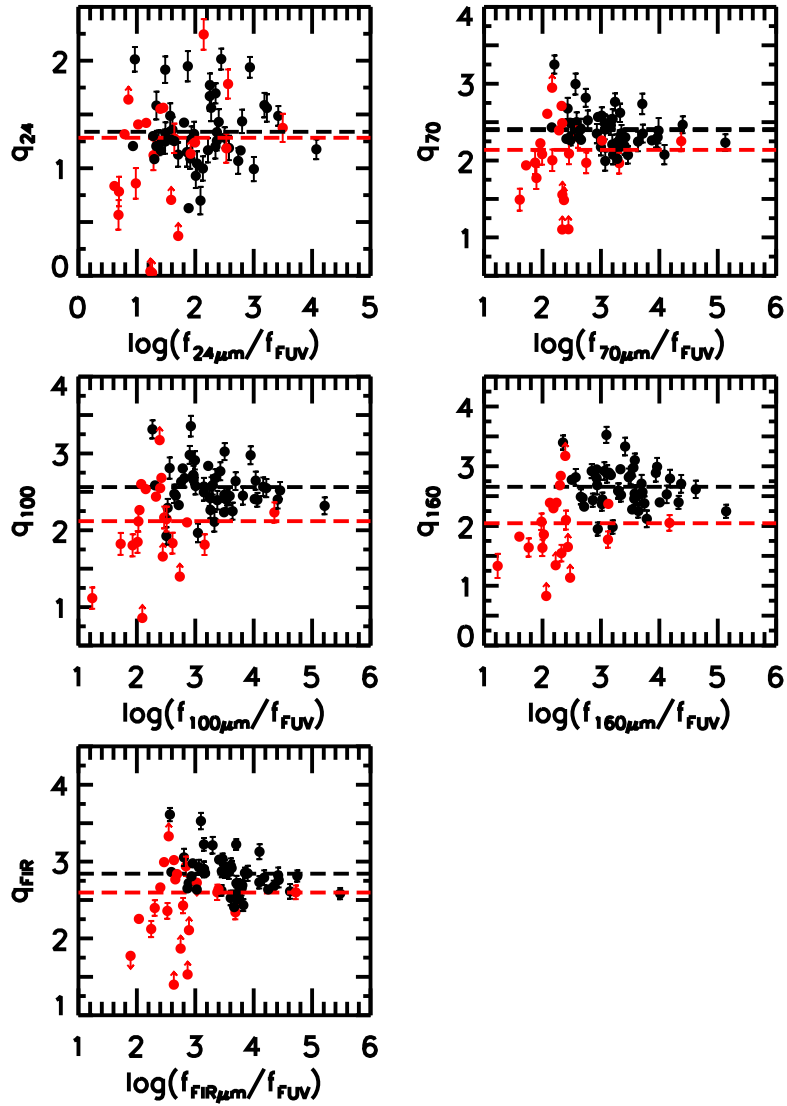


Figure 4. The q_{IR} as a function of the IR-to-FUV ratio at corresponding IR wavelength. The red points denote metal-poor galaxies and black points are for metal-rich galaxies. The two horizontal dashed lines indicate the average values of metal-poor and metal-rich galaxies, respectively.

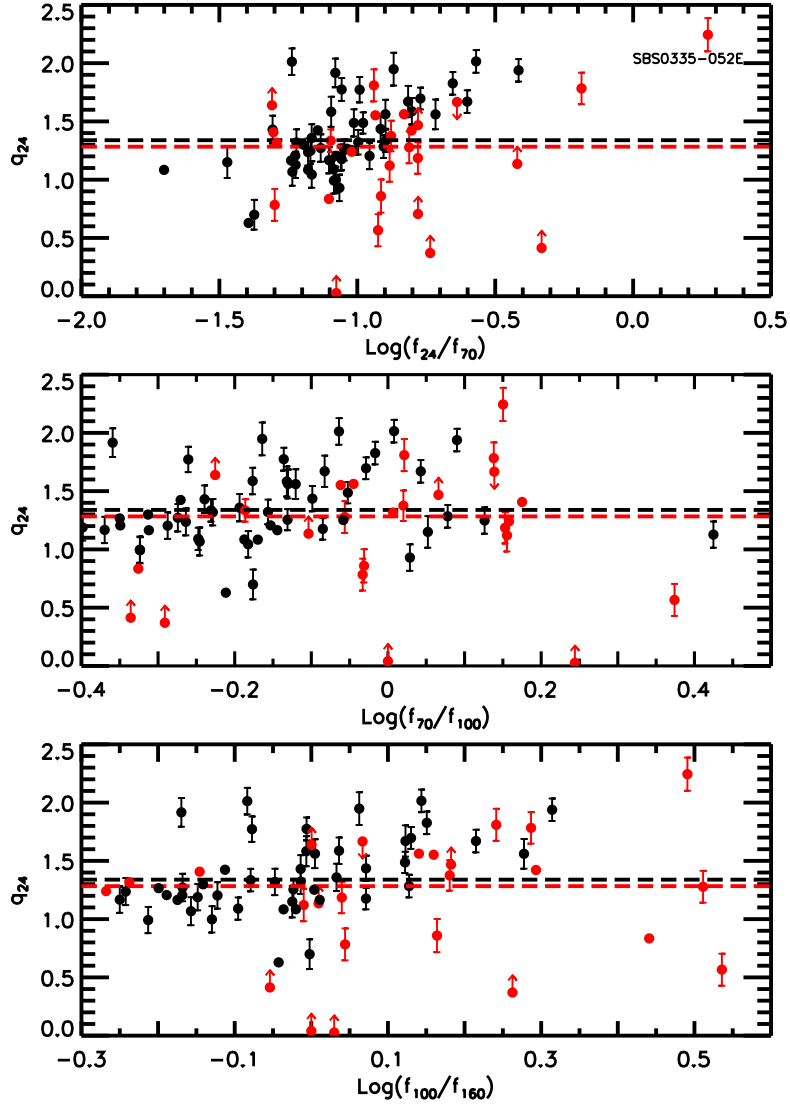


Figure 5. $q_{24\mu\text{m}}$ vs. the IR color of $f_{24\mu\text{m}}/f_{70\mu\text{m}}$, $f_{70\mu\text{m}}/f_{100\mu\text{m}}$ and $f_{100\mu\text{m}}/f_{160\mu\text{m}}$. The red points denote metal-poor galaxies and black points are for metal-rich galaxies. The two horizontal dashed lines indicate the average values of metal-poor and metal-rich galaxies, respectively.

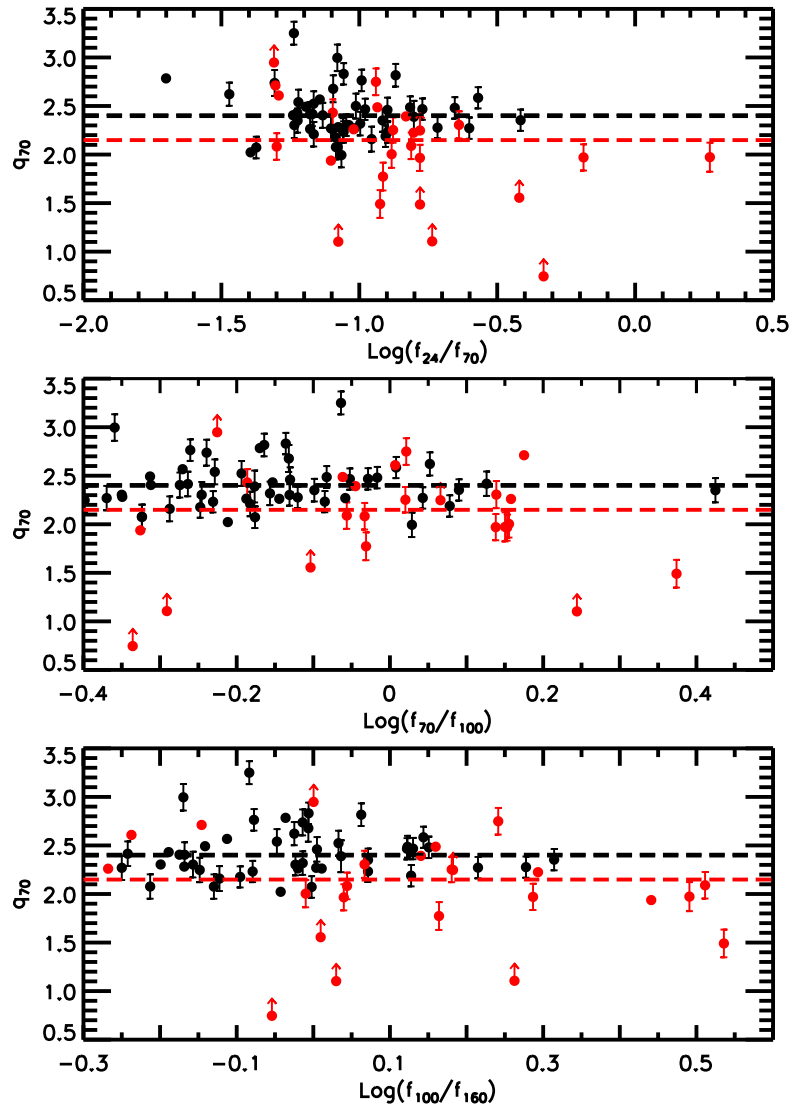


Figure 6. The same as Fig. 5 but for $q_{70\mu\text{m}}$.

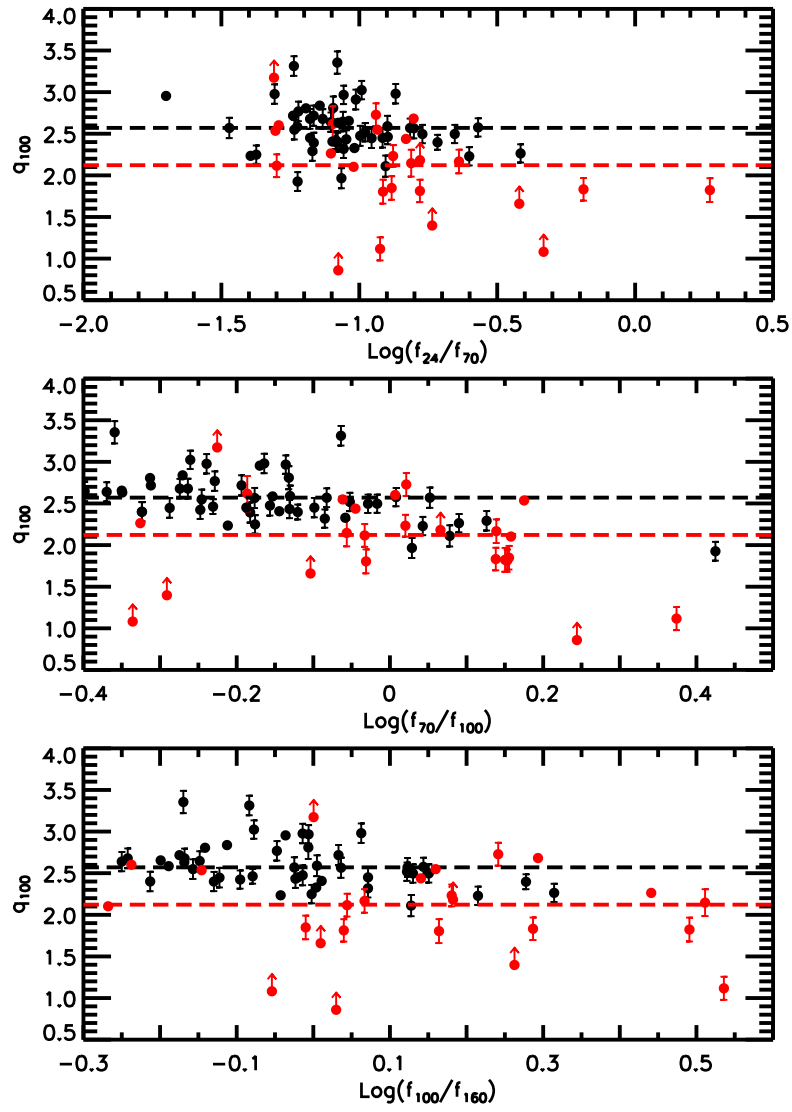


Figure 7. The same as Fig. 5 but for $q_{100\mu\text{m}}$.

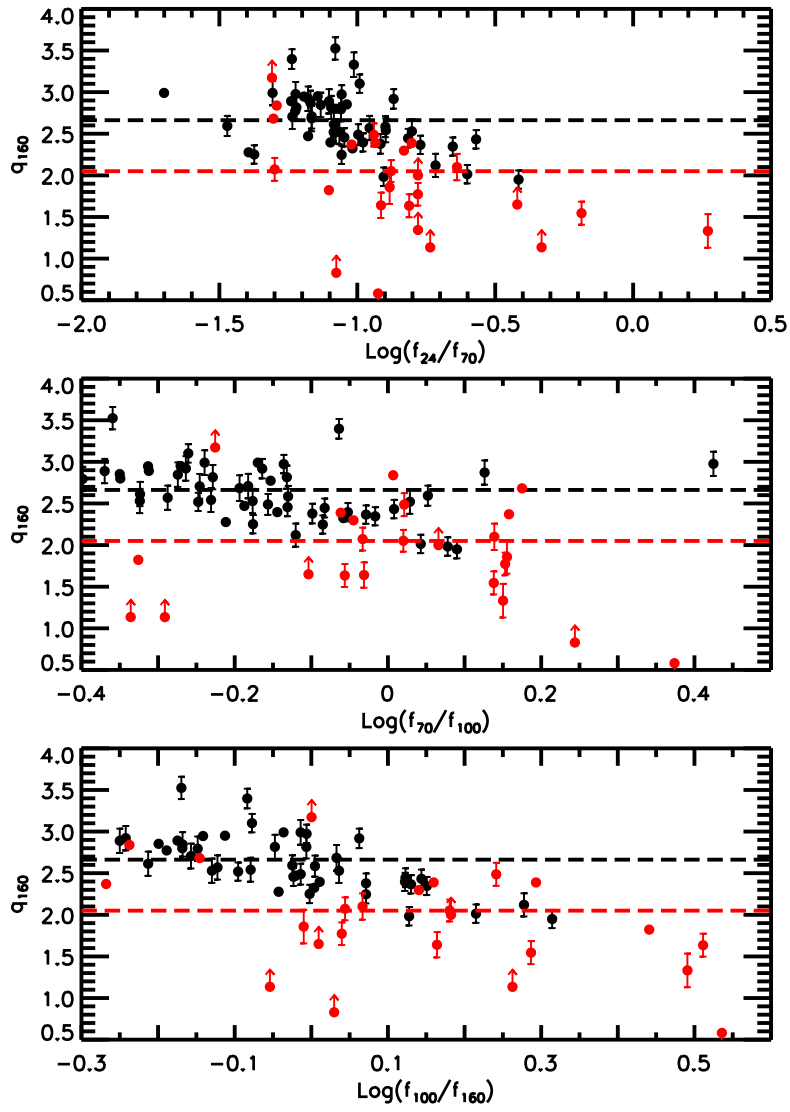


Figure 8. The same as Fig. 5 but for $q_{160\mu\text{m}}$.

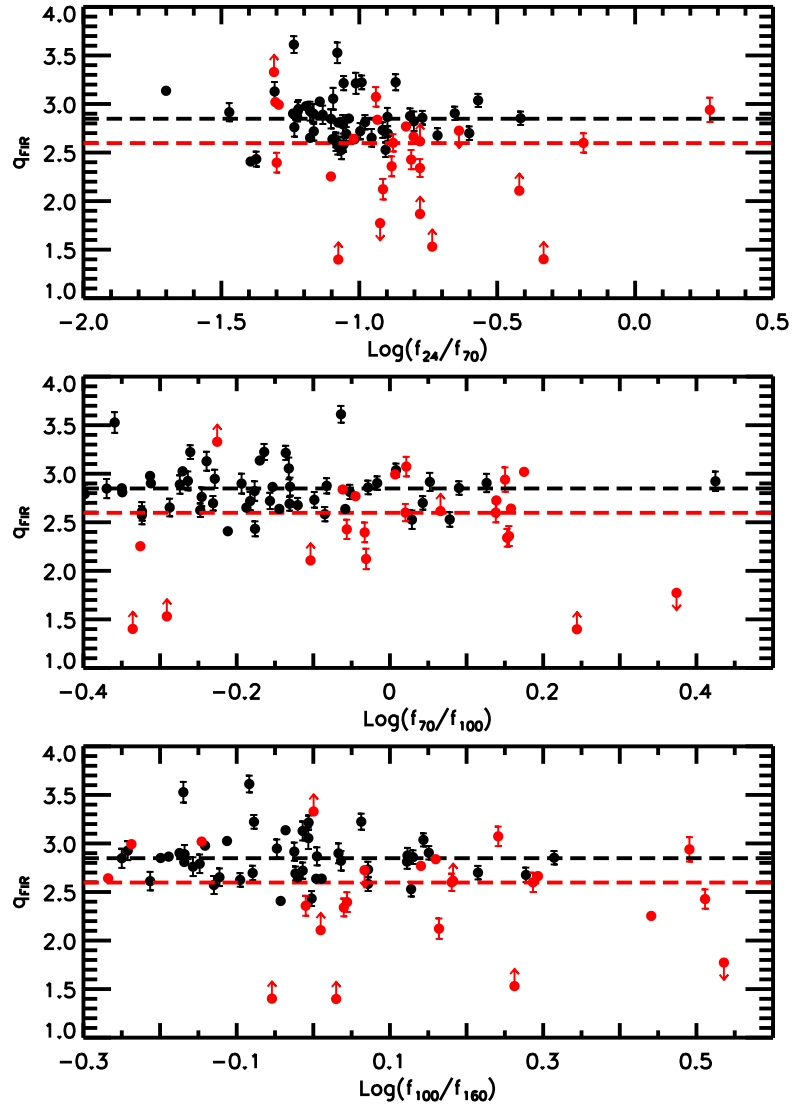


Figure 9. The same as Fig. 5 but for q_{FIR} .

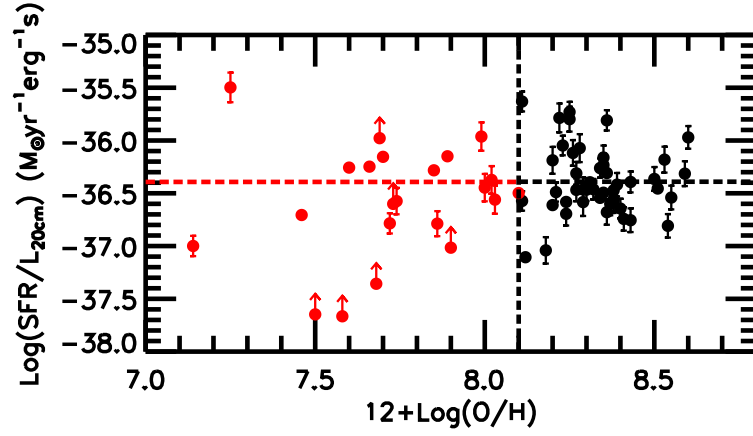


Figure 10. The SFR-to-radio ratio as a function of the oxygen abundance, where the SFR includes both obscured and unobscured contributions.

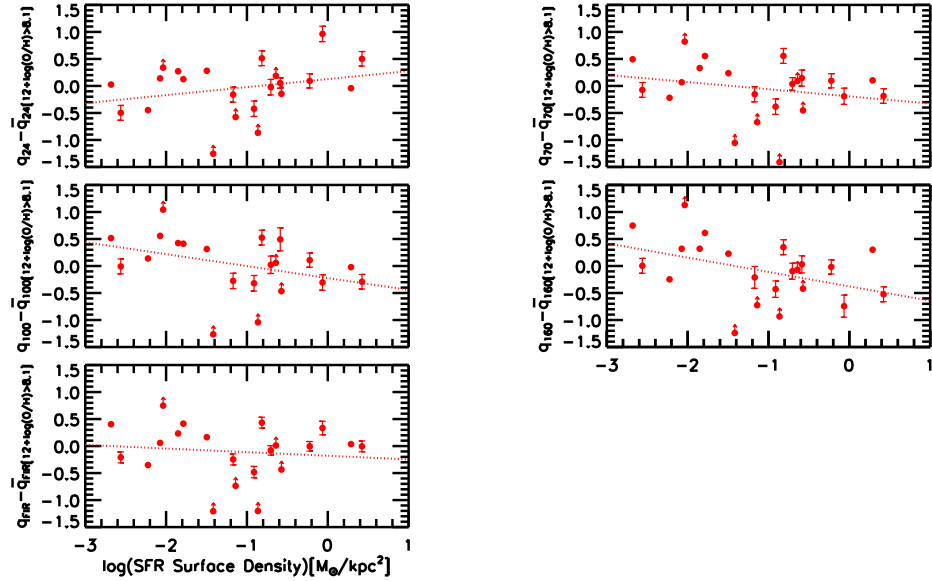


Figure 11. The deviation of q_{IR} of metal-poor galaxies from the mean of metal-rich galaxies as a function of the SFR surface densities. The red dotted line are the best linear fits.

Table 1. The sample of metal-poor galaxies with $12 + \log(\text{O}/\text{H}) < 8.1$.

Name	RA[J2000]	DEC[J2000]	D [Mpc]	FUV ^a [mJy]	REF ^b	20cm ^c [mJy]	REF ^d	12+(O/H)	REF ^e	SFR [M _⊙ /yr]	Σ _{SFR} [M _⊙ /yr/kpc ²]
SBS0335−052E	03h37m44.06s	−05d02m40.0s	56.0	0.579±0.0192	1	0.46±0.061	H04	7.25±0.01	1,6	8.25±2.43	0.86
NGC1569	04h30m49.06s	+64d50m53.0s	3.10	2.56±0.024	2	339±11	C98	8.02±0.02	1,11	2.47±0.74	0.59
Mrk1089	05h01m37.76s	−04d15m28.0s	56.6	5.56±0.56	...	31.7	H02	8.10±0.08	1,13	57.9±16.9	1.89
NGC2366	07h28m54.66s	+69d12m57.0s	3.20	28.1±1.03	2	19.9	C02	7.70±0.01	1,16	0.26±0.07	0.014
IC2233	08h13m58.91s	+45d44m31.7s	9.48	2.81±0.0258	2	<1	L05	7.69±0.00	39	0.17±0.04	0.0086
HolmbergII	08h19m04.98s	+70d43m12.1s	3.28	38.0±0.35	2	30.9±3	VLA	7.72±0.14	5	0.10±0.02	0.0028
DDO053	08h34m07.20s	+66d10m54.0s	3.31	2.01±0.019	2	1.1	L05	7.60±0.11	5	0.012±0.003	0.0084
UGC4483	08h37m03.00s	+69d46m31.0s	3.20	1.82±0.084	3	1.1	H02	7.46±0.02	1,19	0.004±0.0007	0.006
IZw18	09h34m02.03s	+55d14m28.0s	18.2	1.36±0.013	2	1.79±0.18	C05	7.14±0.01	1,22	0.11±0.02	...
SBS0940+544	09h44m16.61s	+54d11m34.3s	23.0	0.148±0.015	...	<2.3	H02	7.50±0.00	17,23	0.049±0.015	...
IC2574	10h28m23.48s	+68d24m43.7s	3.56	3600±33	2	10.7	C02	7.85±0.14	5	0.13±0.03	0.002
Mrk153	10h49m05.03s	+52d20m08.0s	40.3	2.98±0.0624	1	4.50±0.6	C98	7.86±0.04	1,26	2.14±0.51	0.12
VII Zw403	11h27m59.90s	+78d59m39.0s	4.50	2.91±0.0268	2	1.2	T04	7.66±0.01	1,27	0.025±0.006	0.016
Mrk1450	11h38m35.78s	+57d52m27.0s	19.8	<2	H02	7.84±0.01	1,28	0.74±0.22*	0.23
UM461	11h51m33.35s	−02d22m22.0s	13.2	0.525±0.0484	4	<2.6	H02	7.73±0.01	1,26	0.20±0.06	0.27
UM462	11h52m37.19s	−02d28m09.9s	13.4	2.77±0.255	4	6.4±0.6	C98	8.00±0.00	17,35	0.74±0.21	0.21
SBS1159+545	12h02m02.47s	+54d15m50.0s	57.0	<2.3	H02	7.44±0.01	1,28	0.62±0.19*	0.14
SBS1211+540	12h14m02.58s	+53d45m17.0s	19.3	0.169±0.0098	1	<2.9	H02	7.58±0.01	1,28	0.04±0.01	1.86
Mrk209	12h26m15.92s	+48d29m37.0s	5.80	3.08±0.142	3	4.5±0.5	C98	7.74±0.01	1,27	0.07±0.02	0.068
SBS1249+493	12h51m52.50s	+49d03m28.0s	111	0.101±0.01	...	<2.2	H02	7.68±0.02	1,32	2.14±0.61	...
SHOC391	12h53m05.97s	−03d12m58.9s	99.7	1.00±0.034	1	6±0.5	C98	7.99±0.02	40	117±35	2.22
NGC4861	12h59m02.34s	+34d51m34.0s	7.50	12.9±0.12	2	10	T04	7.89±0.01	1,27	0.72±0.20	0.032
NGC5408	14h03m20.91s	−41d22m39.7s	4.87	6.53±0.661	VLA	7.81±0.09	5	0.31±0.09*	0.15
Mrk475	14h39m05.46s	+36d48m21.9s	11.2	0.334±0.014	1	<2.7	H02	7.90±0.00	17,35	0.059±0.017	0.072
SBS1533+574	15h34m13.80s	+57d17m06.0s	54.2	0.7±0.07	...	1.4±0.159	FIRST	8.05±0.01	1,27	< 6.28	...
Mrk1499	16h35m21.00s	+52d12m52.3s	39.0	1.49±0.142	FIRST	8.10±0.00	17,37	1.57±0.31*	0.26
Mrk930	23h31m58.39s	+28h56m49.9s	77.8	0.589±0.0543	4	13.1±1	C98	8.03±0.01	1,6	39.2±11.7	...

^a Far-ultraviolet flux.^b (1) Galaxy Evolution Explorer (GALEX) All-Sky Catalog based on GALEX General Release 6; (2) Gil de Paz et al. (2007); (3) Lee et al. (2011); (4) Brown et al. (2014); (5) Muñoz-Mateos et al. (2009); (6) Hao et al. (2011)^c 20 cm radio continuum emission flux.^d The reference of 20cm flux: C02 (Condon et al. 2002); C98 (Condon et al. 1998); K91 (Klein et al. 1991); H02 (Hopkins et al. 2002); H94 (Hunter et al. 1994); H04 (Hunt et al. 2004); C04 (Cannon & Skillman 2004); M08 (Matthews & Uson 2008); L05 (Leroy et al. 2005); C05 (Cannon et al. 2005); T04 (Thuan et al. 2004); Kepley11 (Kepley et al. 2011); H64 (Heeschen & Wade 1964); S76 (Sulentic 1976); VLA (<http://archive.nrao.edu/nvas/>); FIRST (<http://sundog.stsci.edu/index.html>).^e the reference of oxygen abundance: (1) (Rémy-Ruyer et al. 2013); (2) (Magrini & Gonçalves 2009); (3) (Ugrumov et al. 2003); (4) (Guseva et al. 2012); (5) (Moustakas et al. 2010); (6) (Izotov & Thuan 1998); (7) (Skillman et al. 2003); (8) (van Zee et al. 1996); (9) (Kobulnicky et al. 1999); (10) (Izotov et al. 2004); (11) (Kobulnicky & Skillman 1997); (12) (Lee & Skillman 2004); (13) (López-Sánchez et al. 2004); (14) (Guseva et al. 2000); (15) (Masegosa et al. 1994); (16) (Saviane et al. 2008); (17) (Wu et al. 2008); (18) (Pustilnik et al. 2003); (19) (van Zee & Haynes 2006); (20) (Heckman et al. 1998); (21) (Kobulnicky & Johnson 1999); (22) (Izotov et al. 1999); (23) (Thuan & Izotov 2005); (24) (Storchi-Bergmann et al. 1994); (25) (Kong et al. 2002); (26) (Izotov et al. 2006); (27) (Izotov et al. 1997); (28) (Izotov et al. 1994); (29) (Izotov et al. 2007); (30) (McCall et al. 1985); (31) (Popescu & Hopp 2000); (32) (Thuan et al. 1995); (33) (Guseva et al. 2007); (34) (Guseva et al. 2003); (35) (Izotov & Thuan 1999); (36) (Guseva et al. 2003); (37) (Shi et al. 2005); (38) (Lee et al. 2006); (39) (Berg et al. 2012); (40) (Esteban et al. 2014).

* SFR estimate without FUV (no FUV archival data).

Table 2. The IR photometry of metal-poor galaxies.

Name	24 μ m [mJy]	70 μ m[mJy] [mJy]	100 μ m[mJy] [mJy]	160 μ m[mJy] [mJy]
SBS0335-052E	81 \pm 8	42 \pm 5	30 \pm 3	10 \pm 2
NGC1569	8038 \pm 804	60628 \pm 6063	57877 \pm 5778	38187 \pm 3820
Mrk1089	551 \pm 55	5776 \pm 580	4015 \pm 402	7438 \pm 786
NGC2366	710 \pm 71	6106 \pm 611	7038 \pm 704	4873 \pm 491
IC2233	44 \pm 4	887 \pm 89	1491 \pm 149	1490 \pm 153
HolmbergII	188 \pm 19	3741 \pm 374	4036 \pm 404	3647 \pm 370
DDO053	29 \pm 3	185 \pm 20	529 \pm 54	269 \pm 40
UGC4483	7.5 \pm 0.8	95 \pm 10	201 \pm 21	73 \pm 15
IZw18	6.6 \pm 0.7	55 \pm 6	23 \pm 2	<6.8
SBS0940+544	2.5 \pm 0.4
IC2574	222 \pm 22	4343 \pm 436	4275 \pm 429	7384 \pm 752
Mrk153	33 \pm 3	267 \pm 27	287 \pm 30	197 \pm 24
VII Zw403	31 \pm 3	617 \pm 65	412 \pm 44	577 \pm 124
Mrk1450	59 \pm 6	354 \pm 36	304 \pm 31	200 \pm 23
UM461	35 \pm 4	93 \pm 9	119 \pm 13	116 \pm 15
UM462	121 \pm 12	787 \pm 79	896 \pm 143 ^I	276 \pm 28
SBS1159+545	6 \pm 0.6	13 \pm 3	28 \pm 4	31 \pm 7
SBS1211+540	3 \pm 0.3	37 \pm 4	21 \pm 3	20 \pm 5
Mrk209	59 \pm 6	454 \pm 47	317 \pm 34	325 \pm 82
SBS1249+493	5 \pm 0.5	28 \pm 4	55 \pm 7	30 \pm 8
SHOC391	364 \pm 36	560 \pm 56	408 \pm 41	211 \pm 23
NGC4861	365 \pm 36	2471 \pm 247	2740 \pm 274	1983 \pm 200
NGC5408	421 \pm 42	3664 \pm 367	3489 \pm 349	2002 \pm 204
Mrk475	14 \pm 1	83 \pm 12	...	60 \pm 14
SBS1533+574	<65	283 \pm 29	205 \pm 22	176 \pm 26
Mrk1499	32.2 ^I	402 \pm 40	617 \pm 173 ^I	...
Mrk930	201 \pm 20	1211 \pm 121	851 \pm 86	777 \pm 80

^I Taken from IRAS.

Table 3. The comparison sample of metal-rich galaxies with $12 + \log(\text{O}/\text{H}) > 8.1$.

Name	D [Mpc]	3.6 μm [Jy]	24 μm [Jy]	70 μm [Jy]	100 μm [Jy]	160 μm [Jy]	FUV [mJy]	REF	20cm [mJy]	REF	12+log(O/H)	REF
IC10	0.7	...	2.79 \pm 0.17	140 \pm 7	207 \pm 10	225 \pm 11	230	C02	8.17 \pm 0.03	1,2
Haro11	92.1	22.6 \pm 0.678	2.36 \pm 0.0473	6.14 \pm 0.31	4.99 \pm 0.25	2.42 \pm 0.12	2.74 \pm 0.0225	1	27.2 \pm 0.9	C98	8.36 \pm 0.01	1,4
NGC0337	21	98.6 \pm 0.227	0.55 \pm 0.0506	13 \pm 0.7	19.5 \pm 1	19.6 \pm 1	4.48 \pm 0.0205	1	110 \pm 4.1	C98	8.18 \pm 0.07	5
UM311	23.5	2.94 \pm 0.15	5.63 \pm 0.28	6.1 \pm 0.31	8.36 \pm 0.01	1,6
NGC625	3.9	123 \pm 17	0.879 \pm 0.095	6.49 \pm 0.32	9.47 \pm 0.47	8.2 \pm 0.41	11.8 \pm 0.544	3	9.9 \pm 1	C04	8.22 \pm 0.02	1,7
NGC0855	9.73	42.6 \pm 0.294	0.0777 \pm 0.00715	2.30 \pm 0.12	2.04 \pm 0.12	2.16 \pm 0.12	1.08 \pm 0.01	2	5.5 \pm 0.6	C98	8.29 \pm 0.10	5
NGC0925	8.58	321 \pm 1.48	0.899 \pm 0.0145	10.8 \pm 0.6	24.7 \pm 1.2	36.5 \pm 1.8	29.4 \pm 0.271	2	10.9 \pm 2	C98	8.25 \pm 0.01	5
NGC1097	17.1	1240 \pm 170	6.63 \pm 0.27	59.84 \pm 4.66	116 \pm 6	153.8 \pm 18.5	29.9 \pm 1.1	2	415 \pm 42	D07	8.55 \pm 0.09	5
NGC1140	20	...	0.388 \pm 0.00782	4.04 \pm 0.2	4.62 \pm 0.23	4.58 \pm 0.23	8.87 \pm 0.0817	2	21.7	H94	8.38 \pm 0.01	1,10
NGC1482	19.6	201 \pm 1.86	3.57 \pm 0.0329	40.7 \pm 2	49.5 \pm 2.5	42 \pm 2.1	0.302 \pm 0.0222	2	238 \pm 8.4	C98	8.11 \pm 0.13	5
NGC1705	5.1	27.3 \pm 0.126	0.056 \pm 0.002	1.37 \pm 0.07	1.46 \pm 0.07	1.1 \pm 0.06	13.6 \pm 0.0886	1	8.27 \pm 0.11	1,12
II Zw40	12.1	16 \pm 0.481	1.6 \pm 0.032	6.39 \pm 0.32	5.79 \pm 0.29	3.53 \pm 0.18	34.2 \pm 1.4	C98	8.23 \pm 0.01	1,14
NGC2403	3.13	1880 \pm 250	5.84 \pm 0.24	86.36 \pm 6.18	64.59 \pm 3.23	245.6 \pm 29.6	192 \pm 1.77	2	330 \pm 33	D07	8.3 \pm 0.14	5
UGC4274	6.9	80.8 \pm 2.43	0.276 \pm 0.0254	4.04 \pm 0.203	6.31 \pm 0.2	5.85 \pm 0.703	6.79 \pm 0.0626	2	12.1 \pm 1.9	M08	8.5	17
He2-10	8.7	97.4 \pm 2.92	5.68 \pm 0.114	25.6 \pm 1.3	26.6 \pm 1.3	18.8 \pm 0.9	84.7 \pm 3.4	C98	8.43 \pm 0.01	1,9
NGC2798	26.4	69.2 \pm 0.319	2.54 \pm 0.0176	24.2 \pm 1.2	27.3 \pm 1.4	20.6 \pm 1	0.964 \pm 0.00888	2	82.8 \pm 3	C98	8.34 \pm 0.08	5
NGC2903	8.9	1130 \pm 33.9	9.69 \pm 0.194	76.4 \pm 3.83	130 \pm 0.2	156 \pm 20.3	41.3 \pm 0.38	2	448 \pm 14	C98	9.3	17,21
NGC2976	3.95	408 \pm 0.94	1.38 \pm 0.00317	19.2 \pm 1	35.8 \pm 1.8	46.4 \pm 2.3	21.5 \pm 1.58	2	52	C02	8.36 \pm 0.06	5
NGC3049	24.8	41.1 \pm 0.0947	0.43 \pm 0.02	3.40 \pm 0.18	4.59 \pm 0.23	4.54 \pm 0.24	2.3 \pm 0.00373	1	11.8 \pm 1.7	C98	8.53 \pm 0.01	5
NGC3031	3.55	10920 \pm 1480	5.09 \pm 0.2	85.18 \pm 5.96	32.03 \pm 1.28	360 \pm 43.4	100 \pm 0.921	2	380 \pm 38	D07	8.37 \pm 0.14	5
HoIX	3.7	7 \pm 1	0.004 \pm 0.0006	0.054 \pm 0.014	...	0.204 \pm 0.041	2.27 \pm 0.0209	2	8.14 \pm 0.11	5
NGC3077	3.8	496 \pm 14.9	1.79 \pm 0.0362	20.4 \pm 1	27.9 \pm 1.4	28.3 \pm 1.4	30.1 \pm 1.5	C98	8.6	17,24
NGC3184	12.2	515 \pm 1.19	1.42 \pm 0.00327	15.5 \pm 0.8	34.7 \pm 1.7	54.9 \pm 2.8	37.1 \pm 0.0684	5	77	C02	8.51 \pm 0.01	5
NGC3198	14	270 \pm 0.621	0.561 \pm 0.0517	9.75 \pm 0.51	20 \pm 1	29.9 \pm 1.5	21.7 \pm 0.2	2	38.4	C02	8.34 \pm 0.02	5
NGC3265	1.6	25.4 \pm 0.117	0.3 \pm 0.01	2.47 \pm 0.13	3.1 \pm 0.16	2.63 \pm 0.15	0.474 \pm 0.00437	2	11 \pm 1	C98	8.27 \pm 0.14	5
Haro2	21.7	26.1 \pm 0.18	0.845 \pm 0.00973	4.99 \pm 0.25	5.33 \pm 0.27	3.95 \pm 0.2	3.8 \pm 0.035	2	17 \pm 0.7	C98	8.23 \pm 0.03	1,25
NGC3351	10.1	773 \pm 1.78	2.58 \pm 0.12	25.3 \pm 1.3	46.1 \pm 2.3	55.1 \pm 2.8	14.5 \pm 0.133	2	43.6 \pm 2	C98	8.60 \pm 0.01	5
Haro3	19.3	...	0.81 \pm 0.081	5.30 \pm 0.26	6.41 \pm 0.32	4.83 \pm 0.24	4.57 \pm 0.0421	2	17.3 \pm 1.3	C98	8.28 \pm 0.01	1,10
NGC3521	10.1	2050 \pm 280	5.51 \pm 0.22	63.13 \pm 4.54	158 \pm 8	222.3 \pm 26.8	14.6 \pm 0.134	2	357 \pm 36	D07	8.38 \pm 0.11	5
NGC3621	6.55	990 \pm 130	3.7 \pm 0.19	50.21 \pm 3.94	94.4 \pm 4.7	139 \pm 17.1	42.9 \pm 1.97	2	198 \pm 20	D07	8.29 \pm 0.14	5
NGC3773	17	22.2 \pm 0.307	0.13 \pm 0.003	1.29 \pm 0.08	1.85 \pm 0.11	1.91 \pm 0.14	4.22 \pm 0.0311	5	6.2 \pm 0.6	C98	8.43 \pm 0.03	5
UM448	87.8	14.5 \pm 0.434	0.644 \pm 0.0129	5.17 \pm 0.26	4.32 \pm 0.389	3.22 \pm 0.17	2.03 \pm 0.0209	1	33.5 \pm 1.4	C98	8.32 \pm 0.01	1,6
NGC4194	41.5	94.8 \pm 2.84	3.67 \pm 0.338	19.1 \pm 0.953	25.2 \pm 0.11	13.3 \pm 1.59	2.18 \pm 0.2	4	101 \pm 3.1	C98	8.2	17,24
NGC4214	2.9	312 \pm 9.37	1.97 \pm 0.0395	24.5 \pm 1.2	33.2 \pm 1.6	33.7 \pm 1.7	91.2 \pm 4.2	3	51.5 \pm 10.3	K11	8.26 \pm 0.01	1,9
NGC4254	16.5	700 \pm 100	4.2 \pm 0.17	50.29 \pm 3.6	106 \pm 5	142.9 \pm 17.2	31.1 \pm 1.46	6	422 \pm 42	D07	8.41 \pm 0.14	5
NGC4321	14.32	950 \pm 130	3.34 \pm 0.13	40.59 \pm 2.9	85.5 \pm 4.3	139.6 \pm 16.8	3.32 \pm 0.0266	1	340 \pm 34	D07	8.43 \pm 0.08	5
NGC4449	4.2	493 \pm 14.8	3.27 \pm 0.0655	49.3 \pm 2.5	75.9 \pm 3.8	79.5 \pm 4	164 \pm 7.57	3	269	C02	8.2 \pm 0.11	1,30
NGC4536	15.3	418 \pm 2.89	3.49 \pm 0.0161	38.9 \pm 2	52.6 \pm 2.6	55.5 \pm 2.8	14.9 \pm 0.137	2	194 \pm 7.6	C98	8.21 \pm 0.08	5
NGC4559	10.3	350 \pm 50	1.12 \pm 0.05	16.89 \pm 1.2	31 \pm 1.6	54.15 \pm 6.53	47.4 \pm 0.437	2	65 \pm 7	D07	8.27 \pm 0.10	5
NGC4625	8.2	49.7 \pm 0.8	0.114 \pm 0.0105	1.36 \pm 0.12	3.04 \pm 0.2	4.48 \pm 0.23	5.3 \pm 0.0488	2	7.1	C02	8.35 \pm 0.17	5
NGC4631	5.83	1190 \pm 2.75	5.53 \pm 0.509	137 \pm 7	223 \pm 11	246 \pm 12	71.8 \pm 0.661	2	1300	C98	8.12 \pm 0.11	5
NGC4725	11.91	1140 \pm 150	0.86 \pm 0.04	8.85 \pm 0.66	22.8 \pm 1.2	59.91 \pm 7.36	23.1 \pm 0.107	5	28 \pm 3	D07	8.35 \pm 0.13	5
NGC4736	5.2	3600 \pm 490	5.65 \pm 0.23	93.93 \pm 7.34	159 \pm 8	177.4 \pm 21.4	59.2 \pm 0.545	2	271 \pm 27	D07	8.39 \pm 0.08	5
NGC4826	7.48	2520 \pm 340	2.72 \pm 0.15	55.16 \pm 5.05	95.7 \pm 4.8	98.82 \pm 12.67	10.8 \pm 0.0992	2	101 \pm 10	D07	8.59 \pm 0.11	5
NGC5033	14.8	640 \pm 90	1.97 \pm 0.08	28.81 \pm 2.09	43.85 \pm 2.63	91.07 \pm 11.2	18.4 \pm 0.017	5	178 \pm 18	D07	8.24 \pm 0.24	5
NGC5055	7.8	2380 \pm 320	5.73 \pm 0.23	72.57 \pm 5.16	170 \pm 8	302.3 \pm 36.6	34.7 \pm 0.319	5	390 \pm 39	D07	8.38 \pm 0.18	5
NGC5194	7.62	2660 \pm 360	12.67 \pm 0.53	147.1 \pm 10.6	137.7 \pm 8.26	494.7 \pm 59.8	124 \pm 1.14	2	1490 \pm 150	D07	8.54 \pm 0.09	5
NGC5253	4	255 \pm 7.64	8.87 \pm 0.177	32.9 \pm 1.6	32.3 \pm 1.6	23.2 \pm 1.2	31.9 \pm 0.294	2	85.7 \pm 3.4	C98	8.25 \pm 0.02	1,9
NGC5474	5.95	104 \pm 0.241	0.193 \pm 0.00356	3.24 \pm 0.18	4.61 \pm 0.25	7.12 \pm 0.37	22.5 \pm 0.207	2	12	C02	8.31 \pm 0.22	5
NGC5713	22	200 \pm 0.461	2.31 \pm 0.0107	28.9 \pm 1.4	40.3 \pm 2	39.3 \pm 2	3.87 \pm 0.0357	2	158	C02	8.24 \pm 0.06	5
NGC6822	0.5	3080 \pm 92.3	3.18 \pm 0.13	54.9 \pm 2.8	63.6 \pm 3.2	77.1 \pm 3.9	344 \pm 0.316	5	30.9 \pm 3.26	VLA	8.11 \pm 0.01	1,38
NGC6946	5.66	3290 \pm 7.57	20.2 \pm 0.357	246 \pm 12	435 \pm 22	542 \pm 27	246 \pm 0.678	5	1640 \pm 51	S76	8.40 \pm 0.03	5
NGC7331	14.52	1610 \pm 220	4.36 \pm 0.25	74.97 \pm 6.62	132 \pm 7	189.5 \pm 24.3	8.02 \pm 0.0738	2	373 \pm 37	D07	8.36 \pm 0.07	5
NGC7552	21	450 \pm 60	10.66 \pm 0.44	67.59 \pm 11.1	101.5 \pm 6.09	93.39 \pm 11.25	6.98 \pm 0.0643	2	276 \pm 28	D07	8.35 \pm 0.03	5
HS2352+2733	117	0.039 \pm 0.003	0.016 \pm 0.002	0.016	0.0322 \pm 0.00476	1	8.40 \pm 0.10	1,3
NGC7793	3.93	746 \pm 1.72	2.05 \pm 0.00471	32 \pm 1.6	65.8 \pm 3.3	91.1 \pm 4.6	108 \pm 0.991	2	103	C96	8.31 \pm 0.02	5

1, The IR photometry were retrieved from NED as observed by IRAS, Spitzer and Herschel with the references including Dale et al. (2007, 2009, 2012); Engelbracht et al. (2008); Muñoz-Mateos et al. (2009).

2, The references for the radio and metallicity data can be found in the Table 1 notes.

Table 4. The mean value of q_{IR} and linear fits of various trends.

name	sample		24 μm	70 μm	100 μm	160 μm	FIR
q	metal-poor	mean	1.28 \pm 0.110	2.14 \pm 0.084	2.12 \pm 0.109	2.05 \pm 0.122	2.60 \pm 0.077
	metal-rich	mean	1.34 \pm 0.046	2.40 \pm 0.036	2.56 \pm 0.042	2.66 \pm 0.049	2.84 \pm 0.036
		offset	0.06 \pm 0.119	0.26 \pm 0.091	0.44 \pm 0.117	0.61 \pm 0.131	0.24 \pm 0.085
q vs 12+log(O/H)	entire	correlation	0.164	0.318	0.417	0.567	0.347
q vs L_{IR}	entire	correlation	0.127	-0.094	0.009	0.262	-0.060
q vs $f_{\text{IR}}/f_{\text{FUV}}$	entire	correlation	0.224	0.052	0.249	0.420	0.037
q vs f_{24}/f_{70}	entire	correlation	0.328	-0.336	-0.417	-0.625	-0.315
q vs f_{70}/f_{100}	entire	correlation	0.200	-0.048	-0.529	-0.431	-0.109
q vs f_{100}/f_{160}	entire	correlation	0.263	-0.208	-0.332	-0.710	-0.294
q- \bar{q} vs SFR surface density	metal-poor	correlation	0.368	-0.182	-0.479	-0.457	-0.018
SFR/ $L_{20\text{cm}}$	metal-poor	mean	-36.394 \pm 0.098				
	metal-rich	mean	-36.390 \pm 0.047				
		offset	0.004 \pm 0.108				

NOTE—Throughout the text, we justified the existence of a weak correlation if the coefficient is between 0.2 and 0.5, and the existence of a good relationship for the coefficient larger than 0.5.